The Superpile Cycle: the mobility of LLSVPs in response to plate tectonics

Abigail Plimmer
plimmerar@cardiff.ac.uk
Cardiff University https://orcid.org/0009-0009-5270-8813
J. Huw Davies
Cardiff University https://orcid.org/0000-0003-2656-0260

Article

Keywords: Mantle circulation, LLSVPs, Supercontinent cycles, Superpiles

Posted Date: May 29th, 2025

DOI: https://doi.org/10.21203/rs.3.rs-6682277/v1

Additional Declarations: There is **NO** Competing Interest.

The Superpile Cycle: the mobility of large low shear velocity provinces in response to plate tectonics.

Abigail Plimmer[1*] and J. Huw Davies[1]

[1*]School of Earth and Environmental Sciences, Cardiff University, Cardiff, CF10 3AT, UK.

*Corresponding author(s). E-mail(s): plimmerar@cardiff.ac.uk;
Contributing authors: daviesjh2@cardiff.ac.uk;

Abstract

The coupling between the surface and deep Earth is fundamental to the dynamics of the planet, yet the nature of these interactions remain poorly understood through space and time. These processes are elusive, in part, because of a lack of constraint on the nature and evolution of two antipodal large low shear-velocity provinces (LLSVPs) near the core-mantle boundary (CMB), and the role they play in mantle circulation. The origins and long-term stability of these features are debated. This study aims to assess the relative stability of LLSVP-like structures in 3D mantle circulation models, through the coupling between these structures, upwellings and downwellings.

The 'superpile cycle', named after its close ties to the supercontinent cycle, depicts the evolution of the deep Earth in response to supercontinent dynamics. Supercontinents assemble with stable subduction girdles and antipodal basal mantle structures, then break apart. During dispersal, as new subduction zones form, slabs induce more complex mantle flow and disrupt the stable degree 2 structure in the lowermost mantle. As subduction zones stabilise, LLSVP-like structures tend back to two antipodal piles, and a new supercontinent may assemble. These findings highlights the cyclical and coupled nature of structures in the deep Earth and at the surface.

Keywords: Mantle circulation, LLSVPs, Supercontinent cycles, Superpiles

1 Introduction

The relationship between Earth's surface and deep interior is one of the most fundamental aspects of mantle dynamics. Many previous studies have shown that the two domains are intrinsically linked (e.g. [1–7]), with slabs transferring cold material from the surface towards the core-mantle boundary (CMB) and, in return, plumes may develop from near the CMB and rise towards the surface. Two large low shear-velocity provinces (LLSVPs) are observed at the base of the mantle, beneath Africa and the Pacific Ocean, using seismology [8, 9]. These have been spatially correlated with hotspots at the Earth's surface. and the edges of LLSVPs have often been invoked as plume-generation zones (e.g. [10–15]). The relationship between downwelling slabs and LLSVPs is less clear, in part because the nature of the LLSVPs is enigmatic. Studies have suggested thermal [16–19], or thermo-chemical [20–24] origins for these structures, and recently, their intrinsic density has also been debated [9, 14, 25, 26]. These models lead to different proposed morphologies, with thermal plume clusters [16, 19], thermochemical superplumes [27–29] or dense piles [23, 30, 31] described across the literature. This lack of consensus regarding the nature of LLSVPs has also raised questions regarding their dynamics, with some studies suggesting these antipodal structures have been stable for hundreds of millions to billions of years [10, 32–36], whilst others indicate that they are mobile along the CMB [37–41]. This study investigates the relationship between LLSVP stability and plate tectonics using 3D spherical mantle circulation models, building upon an extensive body of work (e.g. [13, 41–46]), to investigate the relationships between slabs, piles in the lower mantle, and plumes, synthesising these into a model referred to as 'The Superpile Cycle'.

2 Results

In each of our 3D spherical mantle circulation models (for details see Methods section), the LLSVP-like basal mantle structures (BMSs) comprise a series of clustered linear features, with cylindrical upwellings developing at their confluences (figure 1). These models explore a broad parameter space, including differing CMB temperatures, varying thicknesses and densities of a basal primordial layer, different viscosity structures, plate velocities and plate motion reconstructions implemented as a surface boundary condition. For models with a primordial layer, basal mantle structures are pile-like in morphology, though linear features still form areas of higher topography at the top of the structure. The linearity of BMSs has been observed in previous studies [21, 43], and pile-like morphologies may be attributable to the limited resolution inherent in seismic tomography [18, 19, 22]. Superpiles, as referred to in this study, are so named for a number of reasons. Studies have used the term to familiarly refer to LLSVPs [47] regardless of their proposed morphology and, when considered alongside supercontinent dynamics, the similarity in nomenclature is intended to highlight the close coupling between the two realms. Additionally, when the data is filtered to be consistent with the resolution of seismic tomography, or a basal layer is present, the morphologies of the structures are 'pile-like'. In this study, BMS stability is considered in terms of structure volume, change in shape, and the generation of plumes associated with BMSs.

2.1 Volume stability

For the models where we vary the CMB temperature, primordial layer thickness and primordial layer density, most models exhibit a similar evolution though time, though the absolute volumes increase with hotter CMB temperatures, or a thicker, denser primordial layer (shown by the near parallel lines representing each model in figure B1a, d, e). We attribute this to the increase in material which we determine to be LLSVP-like, given the higher temperatures and different compositions within the primordial layer. Whilst the absolute volumes of BMS material are similar across the simulations with different plate velocities (implemented by different scaling factors) and plate motion histories, their temporal evolutions differ significantly (figure B1b, f). The global length of subduction zones in the plate motion reconstruction [48] show peaks during supercontinental assembly, and troughs during periods of supercontinent dispersal, (shown by the similar patterns between subduction zone length and detrital zircon records which reflect the degree of continental crust preservation, figure 2, inset). When global lengths of subduction zones are cross-correlated to the change in volumes across the models, most models show a correlation with the subduction zone lengths if they are shifted by an average of 160 Myrs (figure 2), representing the time for a slab to sink to a depth where it can affect the volume of the structures (figure B2). There are cyclical alternations between positive and negative correlations, with an average cycle duration of 220 $\pm$ 60 Myrs across most models (calculated from the average time between significant peaks in cross-correlation algorithm; see figure B3 caption for more details), reflecting the average cyclicity of peaks in the global length of subduction zones . Models with thick or dense layers of primordial material (models 014, 015, 018, 019) do not exhibit this same cyclicity, which can be attributed to the rapid volume growth of these structures through time shown in figure B1.

During supercontinent assembly, the development of circum-continental subduction zones may result in the development of antipodal BMSs (figure 3a, b), where material is swept simultaneously beneath the supercontinent and beneath the superocean, localising into two piles. Therefore, the cyclicity of volume change may be considered a response to changes in subduction zone geometries or locations (where peaks in subduction zone length reflect higher degree of supercontinentality with longer, circum-continental trenches compared to periods of peak supercontinent dispersal) , and the 160 Myr time lag reflects the time required for slabs to reach a significant depth to affect the deep Earth (figure B2). The relationship between subduction zone lengths and changes in volume are more cyclical and regular beneath the Pacific (figure 3c, d) whereas the relationship is not statistically significant beneath Africa (as denoted by a p-value of 0.43; figure 3c), which we attribute to the more chaotic flow beneath this region through time. Throughout the plate motion reconstruction, the area where Africa currently resides has exhibited more complex subduction patterns, as material is swept not just by circum-continental slabs but intra-continental subduction as internal oceans have closed throughout different phases of the supercontinent cycle (figure B4) inducing a more complex flow pattern in the mantle.

2.2 Variation in BMS morphology

Simulated seismic velocities near the CMB are smoothed up to a spherical harmonic degree four structure, in line with many global seismic tomography studies of the CMB [e.g. 49–56], such that measured change in shape is most sensitive to long-wavelength variations in mantle flow. At this degree of smoothing, a contour value of -0.3 % Vs anomaly encompasses roughly the same structures as the -1.5 % Vs contour in the raw data (figure 4a). The present day antipodal structure beneath the Pacific and Africa only develops between 300-200 Ma, as material is swept by downwellings associated with the formation of Pangaea, during the period when BMS volume changes rapidly (figure 2). Our simulations better represent the shape of the African LLSVP, compared to the shape of the Pacific (as is common across many geodynamic models [19, 57, 58]), though despite this potential mismatch between the shape of the Pacific LLSVP and the Pacific BMS in these simulations (which may be attributable to potentially distinct evolutions and origins of the two structures [26, 46]), the location of the structure is similar to that observed in the present-day, indicating that the processes involved in these simulations, namely subduction, exert a first-order control on the location of accumulated material in the deep Earth.

The dominant spherical harmonic degree near the CMB shows rapid changes $\sim$ 200 Myr after peaks in subduction zone length (figure 4b). These short-lived ($<$ 50 Myr) deviations from a dominant degree 2 structure in the deep Earth indicate a disturbance to the structures in the lowermost mantle, and point towards a similar subduction-related mechanism as discussed previously. Figure 4c shows three areas of downwelling flow (at the north pole, along the western margin of Pangaea, and along the north-eastern edge of Pangaea) in the deep mantle at 320 Ma, as the dominant spherical harmonic degree of the simulation changes from 3 to 2 (figure 4b). The relationship between subduction length and changes in dominant spherical harmonic degree is best reflected by an average 200 Myr forwards shift in the subduction zone lengths (figure B5), such that slabs have time to sink to the lowermost mantle and induce significant BMS migration to alter the dominant degree.

Our findings suggest that the formation of new subduction zones (and the reorganisation of older ones) disrupts the deep mantle structure, and the BMSs are swept around the CMB to a stable location (where flows converge). In these models, this reorganisation occurs over 10-40 Myrs (from when we observe changes in shape and volume to the change in dominant spherical harmonic degree), which we hereafter refer to as 'rearrangement events'. However, the timings of these events in the simulations (160-200 Myrs after the change in subduction patterns at the surface) are not necessarily representative of the Earth, since the slab sinking rate is dependent on the viscosity structure of the mantle, which is currently poorly constrained.

2.3 Distribution of plumes through space and time

Peaks in plume production occur at $\sim$ 700 Ma and between 550-350 Ma across the simulations (figure 5), corresponding with the peaks in BMS rearrangement (volume change in inset; figure 2, changes in spherical harmon degree; figure 4b). Many previous studies have suggested that plumes form from the convergence of flow in the deep mantle [16, 38, 59, 60], which is supported by this study. The flow which controls the location of BMSs (figure 3a,b and figure 4c) is therefore intrinsically linked to the formation of plumes, and suggests that the two classes of structures are closely related. Most plumes ascend above BMSs in our simulations, and are not limited to the edges of the structures as has been suggested in some previous studies [10–15]. We highlight the 700-600 Ma and 500-400 Ma time intervals in figure 5, where a greater proportion of plumes lie outside of the BMS contours. This may reflect the complex flow in the deep mantle during the rearrangement events, as the BMSs begin to migrate and change morphology rapidly. As slabs induce rearrangement in the lower mantle, there is likely a period where the flow converges away from the location of BMSs, as they have not yet had significant time to stabilise in response to the changes in flow. When the behaviour of plumes is considered alongside the stability of BMSs, it is clear that the change in subduction locations have the capacity to impact the entire circulation cycle, and these findings are synthesised into a proposed 'superpile cycle'.

3 Discussion

3.1 The Superpile Cycle

This superpile cycle describes the evolution of the deep mantle from the assembly of a supercontinent, through breakup and towards the assembly of the next supercontinent. The formation of a supercontinent such as Pangaea may be facilitated by the closure of an interior ocean and the formation of circum-continental subduction zones (figure 6, phase 1). At this stage the modelled BMSs, which can be related to real-world LLSVPs, are antipodal. As the supercontinent breaks apart, the circum-continental subduction zones spread, but retain a similar geometry to that during assembly, BMSs stabilise and remain beneath the disassembling supercontinent and its antipodal ocean (figure 6, phase 2).

During supercontinent dispersal, new subduction zones begin to develop (which we may be beginning to observe on Earth with the development of Atlantic subduction zones [61–65]). As these slabs descend into the mantle (figure 6, phase 3), the deep Earth undergoes a rearrangement event. Firstly, after $\sim$ 160 Myrs in these models, material is swept laterally near the CMB such that the structures change shape and volume. Rather than subduction promoting volume gain in the BMSs, it may be that the BMSs are hotter than average given the increase in cold slab material, which also shapes the structures. This interpretation does not require us to rule out a primordial layer as the origins for LLSVPs, where the maximum volume would be defined at the beginning of the simulations and constantly decreasing. As material is continually swept into piles, flow converges and plumes develop. During rearrangement events there are slabs in the mantle from both older and younger subduction zones, flow in the deep Earth is likely more complex, and plumes can form away from the tops of BMSs. Given that the dominant spherical harmonic degree changes across the suite of models after the change to BMS volume and shape, there is an additional time required after slabs reach near the CMB for the structures to split or merge, and migrate significantly to induce the change in dominant spherical harmonic degree. As newer subduction zones become established, the flow in the deep Earth settles back towards a degree 2 structure. BMSs are swept back into two antipodal structures, though perhaps in a different location to the previous, and a new supercontinent may assemble. Previous studies have discussed supercontinent-superplume coupling [13, 30, 41, 66–68] in which sinking oceanic lithosphere can stir mantle flow and drive whole mantle circulation. Our study contributes to this work by linking slab sinking to the stability of LLSVP-like structures at the base of the mantle, and these structures need not resemble a superplume morphology but may instead be a cluster of upwellings which form in response to slab flow, with 'superpile' morphologies being the result of both limited seismic tomography and/or the interaction of multiple plume bases.

3.2 Limitations

Since there is much debate as to the properties of LLSVPs, it is difficult to know the optimum approach by which to define these structures in mantle models. This study defines them by a combination of a thermal and Vs anomaly, which results in structures which are similar to tomography data beneath Africa, but are less similar beneath the Pacific. At least some component of this mismatch beneath the Pacific may be attributable to the way in which we define LLSVP-like material, and therefore future work should seek to continue reconciling seismic data with geodynamic models to better understand the evolution of these structures. Additionally, this study is limited by the 1 Gyr plate motion history which reflects the breakup of Rodinia, and the assembly and dispersal of Pangaea, so around 1.5 supercontinent cycles, with increasing levels of uncertainty earlier in the plate motion reconstruction. Whilst this period is long enough to see some cyclical pattern, this could be better constrained with a longer plate motion history, and subsequent refinements to earlier in the reconstructions.

4 Conclusion

This study explored the stability of LLSVP-like structures in 3D mantle models in response to plate tectonics. This approach builds on previous studies to synthesise the evolution of basal mantle structures into a 'superpile cycle', comprising periods of relative stability interspersed with rapid 'rearrangement events' linked to changes in subduction dynamics at the surface. The cyclical nature of these changes in global-scale subduction dynamics are intrinsically linked to the supercontinent cycle, highlighting the coupling between the lithosphere and deep Earth on the greatest spatial and temporal scales. The size of basal mantle structures are dependent on the CMB temperature, and the potential presence of a primordial layer at the base of the mantle. Whilst CMB temperature and the presence of a primordial layer may affect the absolute stability and plume generating capacity of basal mantle structures, the timing of relative stability versus mobility is controlled from the top down.

5 Figures

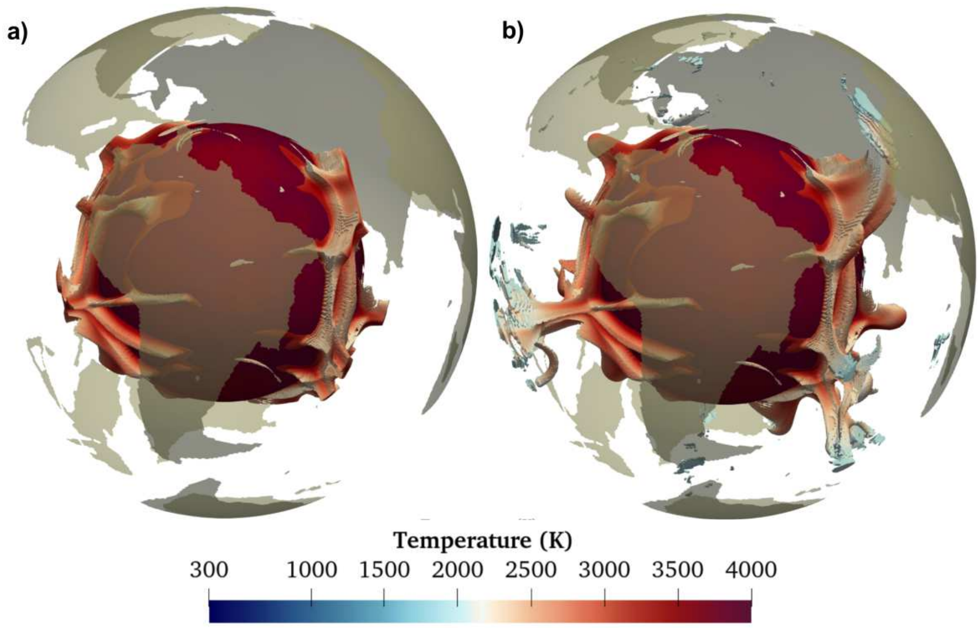

Fig. 1 LLSVP-like basal mantle structures (BMS) as defined by a 200 K temperature anomaly and a -1.5% Vs anomaly, in (a) the bottom 800 km of the mantle, and (b) across the mantle volume for the reference model. Present-day configuration of plates show the location of the basal mantle structures at the end of the simulation.

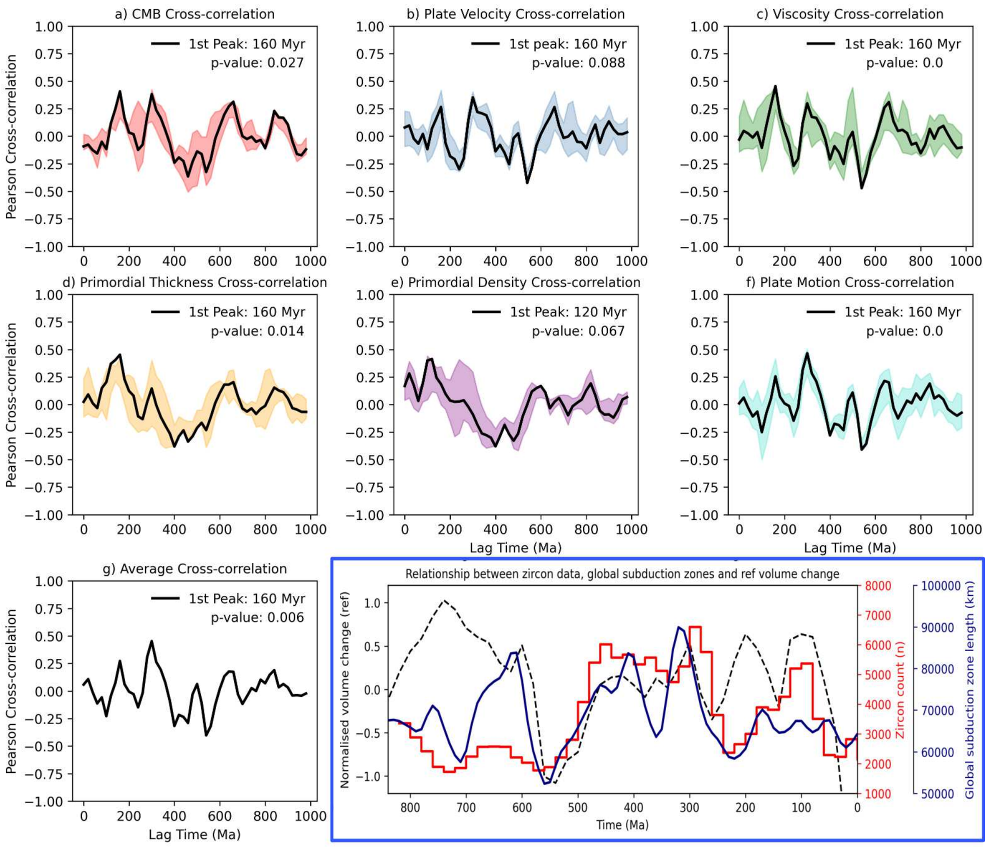

Fig. 2 Results of cross-correlation algorithm showing the relationship between global length of subduction zones and the change in volumes across basal mantle structures through time (inset: global length of subduction zones (blue), detrital zircon records [(red); 69], normalised change in volume from reference model (black). Global subduction zone lengths are shifted forwards by 160 Myrs to show the relationship with normalised volume change. Detrital zircon records are also shifted by 160 Myrs to show the close relationship between subduction zone lengths and supercontinent configuration). (a-f) Black lines show the average cross-correlation for models with different CMB temperatures, plate velocities, viscosities, primordial layer thicknesses, primordial layer densities, and plate motion histories, respectively. Coloured space represents the range of values across each individual model. g) average across all of the models. P-values are calculated from a Monte-Carlo simulation with 1000 iterations, where subduction data is randomly shuffled and compared to the model data.

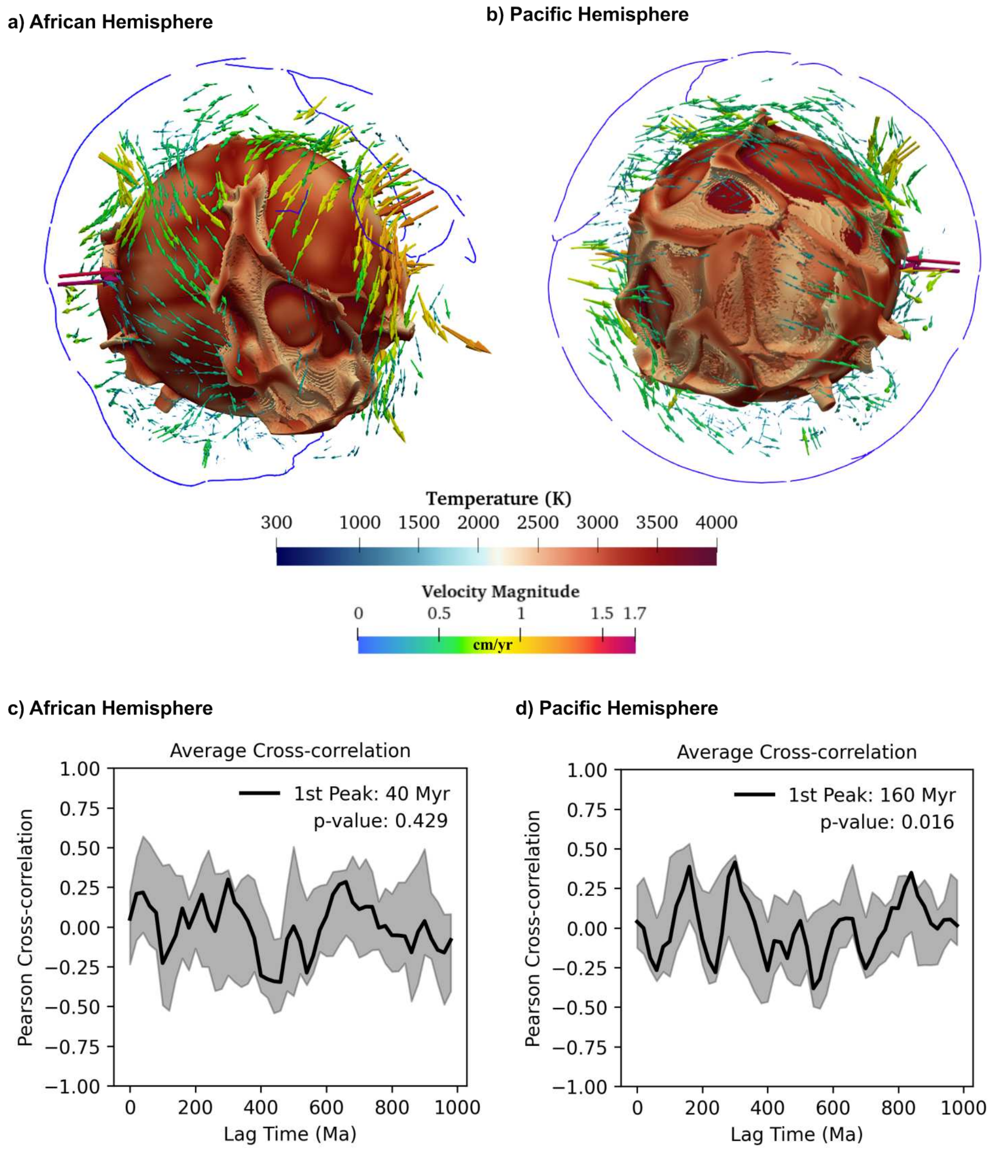

Fig. 3 a) 3D visualisation of accumulation of BMS material in the African hemisphere for model 014 (chosen because of the pile-like morphologies associated with simulations with a primordial layer) at 0Ma, with the locations of subduction zones shown in blue. Arrows show the direction of flow within colder than average mantle material (representing flow associated with downwellings), scaled and coloured by the magnitude of the velocity. b) As with a) but for material accumulated in the Pacific hemisphere. c) Average cross-correlation between subduction zone lengths and BMS volume change beneath the African hemisphere. Grey space reflects the range in correlations across all of the simulations. d) As with c) but beneath the Pacific hemisphere.

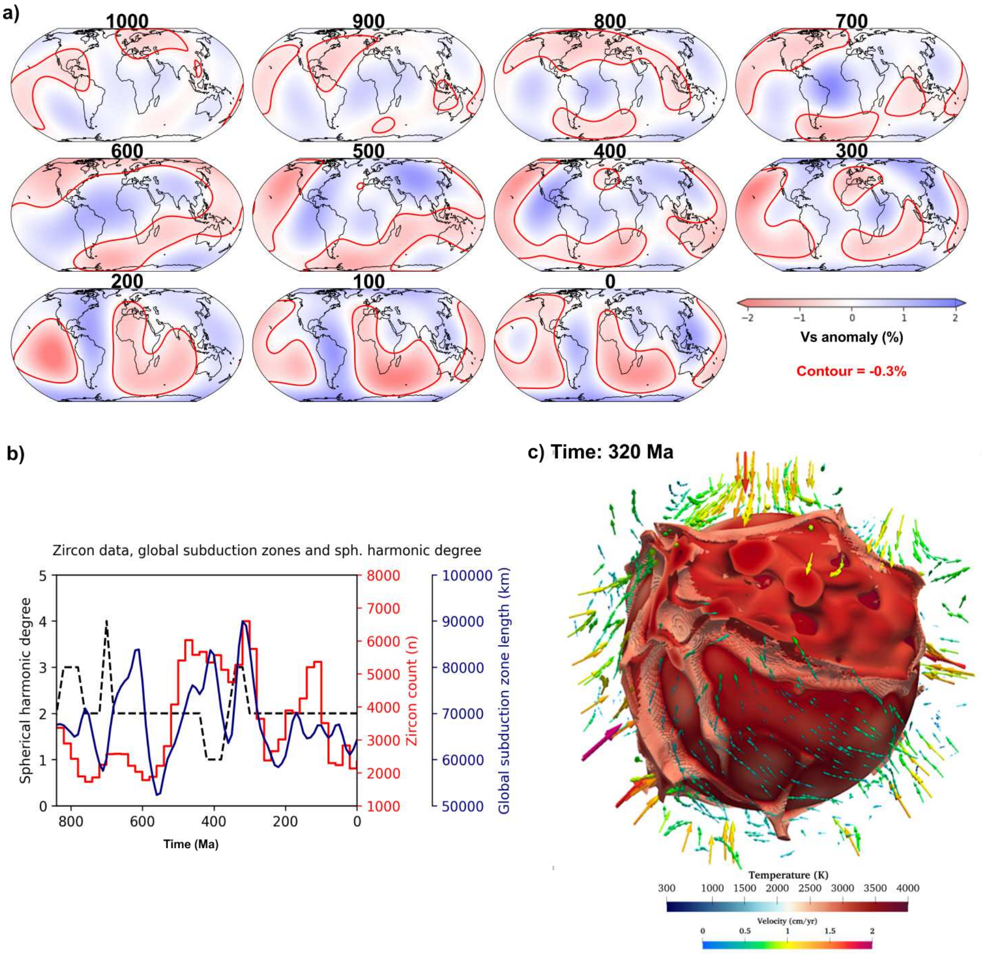

Fig. 4 a) Morphology of the BMSs through time (Ma), contour represents -0.3 % Vs field for data with maximum spherical harmonic degree of 4, at 150 km above the CMB. b) Dominant spherical harmonic degree at 100 km above the CMB (reference model) compared to the global length of subduction zones in the plate motion reconstruction [blue; 48] and detrital zircon data [red; 69], here shifted forwards by 200 Myr; c) 3D visualisation of BMS material for model 014 (chosen because of the pile-like morphology associated with models with primordial layer) at 320 Ma. Arrows show the direction of flow within colder than average mantle material (representing flow associated with downwellings), scaled and coloured by the magnitude of the velocity.

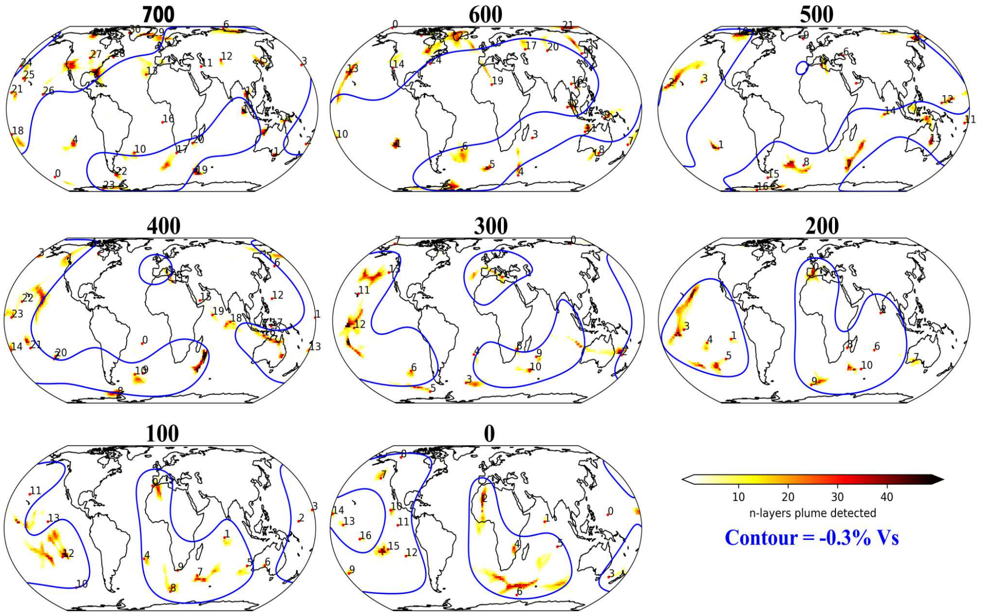

Fig. 5 Location of plumes detected by K-means and density-based clustering between depths of 300-2500 km in reference model. Blue lines reflect the outline of BMSs as defined in figure 4a.

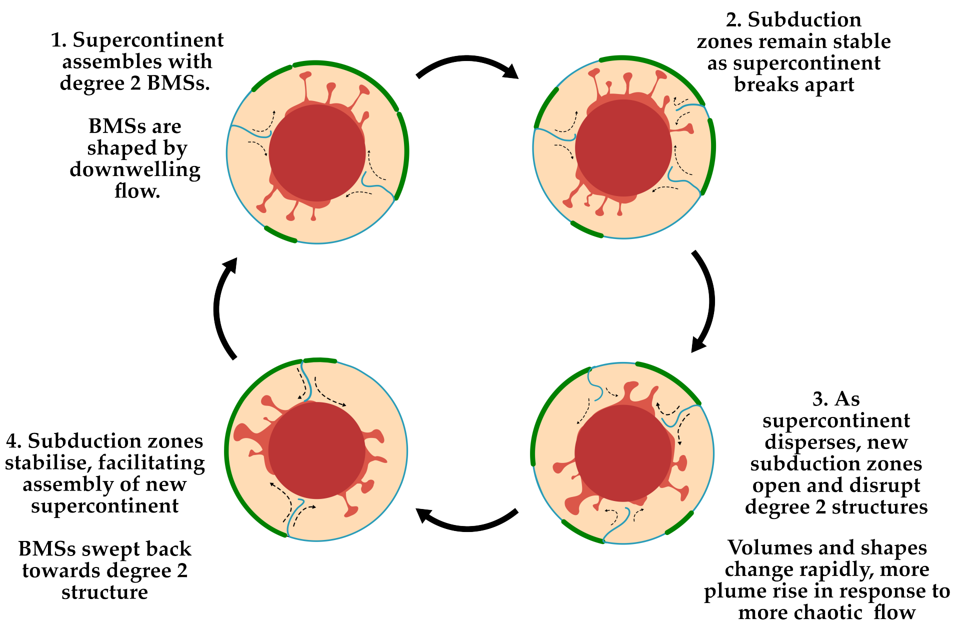

Fig. 6 Schematic representation of the four stages of the proposed superpile cycle. Continental lithosphere is represented in green and oceanic lithosphere is represented in light blue. Dashed arrows reflects the flow associated with downwelling slabs. BMSs form piles above the CMB, with plumes ascending form their tops.

6 Methods

6.1 Reference model

Each of our simulations uses the 3D mantle circulation code, TERRA [70–74]. Calculations are performed on a structured regular mesh based on an icosahedron [75], with over 10 million grid points, an average radial spacing of 45 km, and a lateral spacing of 59.9 km at the model surface which decreases to 32.7 km at the CMB. Our models are compressible, based on the Murnaghan equation of state [72, 76], with isothermal boundary conditions at the surface (300 K) and CMB (4000 K) and internal heating at a rate of 4.0×10^{-12} W kg^{-1}.

Simulations develop from a randomly perturbed temperature field, with a two-layer viscosity structure [where the lower mantle is 30x more viscous than the upper mantle; 77, 78]) and free-slip boundaries at the surface and CMB to allow the initial field to evolve and develop upwellings and downwellings. After 500 Myr of conditioning, we apply surface velocities according to 1000 Myr of plate motion history [48], which comprises a global set of topological plate polygons with associated plate boundaries and velocities at 1 Myr intervals based on a 'mantle reference frame' [79].

As plate velocities are applied, we implement a more complex temperature and depth-dependent viscosity structure with an initial 3-layer radial structure (where the viscosity of the lithosphere is 100x greater than the upper mantle). Temperature-dependence is calculated according to the equation:

$$\mu = \mu_{ir} \cdot e^{(Va \cdot z' - Ea \cdot T')} \quad (1)$$

where μ_{ir} is the reference radial viscosity, Va is the non-dimensionalised constant for activation volume, z' is the non-dimensionalised depth (scaled by mantle depth), Ea is the non-dimensionalised constant for activation energy, and T' is the non-dimensionalised temperature (scaled by the temperature difference between the CMB and surface temperature). For our reference case we use $Va = 1$ and $Ea = 1.5$, representing a mild temperature dependence. Parameters for our reference model are summarised in Table A1.

6.2 Particles, composition, and seismic conversion

To define LLSVP-like structures in these simulations, seismic velocities are calculated based on temperature, pressure, and composition. Whilst the chemical evolution of mantle structures is not a focus of this study, the evolution of composition throughout the simulations are briefly described as it relates to calculating seismic velocities. Further details surrounding the chemical evolution of dynamic models can be found in references [24, 80, 81]. Active particles are used to track chemical compositions throughout the simulations, where bulk composition (C) varies between 0 (depleted; representing harzburgite) and 1 (enriched; representing basalt), with an assumed average composition of $C = 0.2$ (representing lherzolite). Half of particles initialise with a composition of $C = 0.2$, 3/8 with $C = 0.0$, and 1/8 with $C = 1.0$. Melting is controlled by a linear solidus which is dependent on depth (z) and bulk composition [80, 81]:

$$T_{solidus,dry}(z,C) = T_{meltsurf} + zT_{meltslope} + (1-C)T_{meltcomp} \quad (2)$$

where $T_{meltsurf} = 1400$ K is the melting temperature of basalt material at the surface, $T_{meltslope} = 2.5$ K km^{-1} is the gradient of the solidus and $T_{meltcomp} = 500$ K is the difference in solidi temperature between harzburgite and basalt material. The temperature of each particle is linearly interpolated from the grid and if it exceeds the solidus, then it is considered that melting has occurred and the bulk composition is reduced until the particle plots on the solidus for the given temperature and pressure.

To convert particle compositions to seismic velocities, each of the three lithologies (harzburgite, lherzolite, and basalt) are assigned a constant six-oxide composition (Table A2) [82–84], after the methodology outlined in reference [24].

The composition and depth of these particles affects the local density, with basalt being 4% denser than depleted material in the upper mantle, and 3% denser in the lower mantle. This in turn has implications for the buoyancy of the material, calculate according to:

$$B = \frac{\Delta\rho_b}{\rho_0 \Delta T \alpha} \quad (3)$$

where B is the buoyancy, $\Delta\rho_b$ is the density difference between basaltic material and the average composition (C=0.25), ρ_0 is the reference density, ΔT is the temperature difference between the surface and the CMB and α is the coefficient of thermal expansion [85]. The pressures, temperatures, and compositions on each particle are converted to seismic properties using lookup tables for each of the characteristic lithologies. The lookup tables use Gibbs free energy minimisation, as implemented in Perple_X [86] and the associated thermodynamic mineralogical dataset of [87], to calculate values of density and perfectly elastic seismic velocities for each lithology. Attenuation is accounted for using model Q7g [88, 89], in agreement with the data from reference [90]. Seismic velocities are calculated as a post-processing step by taking the harmonic average of harzburgite, lherzolite, and basalt, weighted by the mass fractions of each bulk composition.

6.3 Parameter space

To explore the influence of downwelling dynamics on deep-mantle structures and the potential for these structures to be the sites of plume generation, surface and mantle properties are systematically varied across a suite of 24 models. The uncertainties regarding the role the parameters (CMB temperature [91], mantle viscosity [e.g. 9, 92, 93], and the nature of LLSVPs) play on the intrinsic stability of deep-mantle structures are considered across the parameter space. Therefore, in addition to changing the dynamics of the plate motion at the surface in these simulations, CMB temperature, viscosity structure, and the thickness and density of a basal primordial layer are explored. At the surface, plate velocities are varied by applying a scaling factor (S_v; equation 4), such that the global RMS velocity is reduced by a factor of S_v.

$$S_v = \frac{v_{EARTH}}{v_{MODEL}} \quad (4)$$

In the reference model, this scaling factor is calculated based on the comparison between the average velocity of the plate motion reconstruction (v_{EARTH}) and the natural surface velocities of the pre-conditioning convection solutions (v_{MODEL}). Given that the certainty of published plate motion histories decreases back in time, and there is debate as to the most appropriate reference frame by which to calculate the relative plate motion histories, 5 different plate motion reconstructions are implemented which use different reference frames to explore a wider parameter space of surface dynamics.

The fundamentals of the Müller et al.,[48] plate motion reconstruction are outlined in 6.1. Merdith et al., [94] define the rotation of each plate relative to a palaeomagnetic framework. The model considers the relative movement of plates based on a hierarchy of geological precedence, which is then used with the palaeomagnetic data to iterate towards a solution. Conversely, Cao et al., [42] proposes a global model of relative plate motions, comprising continuously closing polygons and 3 contrasting absolute reference frames; stable supercontinent location (SSL), orthoversion (OV), and no-net-rotation (NNR). SSL considers 3 supercontinents across the last 1 Gyr, all of which occur in the same location as Pangaea. OV is similar in that they are both based on a hybrid of a hotspot track reference frame between 70-0 Ma, and a palaeomagnetic reference frame before 100 Ma [95]. The OV model differs from SSL in that the initial supercontinent is 90° E of Pangaea. Both reference frames minimise net lithospheric rotation whilst the NNR reference frame evaluates the net rotation of the lithosphere with respect to the mantle and removes it from the SSL reconstruction.

The parameter space across this investigation is summarised in Table A3, and viscosity profiles at the beginning and end of each simulation (to show the evolution with temperature dependence) are shown in figure B6.

LLSVP-like material is defined in the simulations by being both +200 K hotter than average and a negative Vs anomaly of no more than -1.5% , extending up to 800 km above the CMB. In the simulations the Vs anomaly is largely dependent on the simulated temperature field, yet both the temperature and Vs thresholds are chosen to define the LLSVP-like material to better constrain the geometry of the structures (since this method excludes some hot material not connected to the CMB). This means that the material deemed to be LLSVP-like can change throughout the simulations and can be recycled through the mantle, as opposed to defining the material at the models initiation and tracking this original material. Plumes are identified using a combination of K-means and density-based clustering performed on the simulated temperature and radial velocity fields [96]. The depth between 300-2500 km is chosen to reduce the effect of the cold surface boundary layer and primordial layers at the base of the mantle, where present.

Acknowledgements. This research was funded by the NERC DTP project 'Constraining the relationship between mantle circulation and supercontinent cycles (Grant No. NE/S007504/1), and completed alongside the work undertaken for the NERC large grant "Mantle Circulation Constrained (MC^2): A multidisciplinary 4D Earth framework for understanding mantle upwellings" (Grant No. NE/T012633/1) and also by the School of Earth and Environmental Sciences, Cardiff University. Numerical simulations were undertaken at (i) ARCHER2, the UK's national high-performance

supercomputers, and (ii) HAWK, part of Supercomputing Wales, the national high-performance supercomputing system for Wales. Plate geometries and plate motion reconstructions utilised GPlates software [97] and 3D visualisations were produced using Paraview [98], and map projections were produced using terratools [96] and the Matplotlib package for Python [99].

Declarations

- Conceptualisation: J. Huw Davies, Abigail Plimmer
- Data curation: Abigail Plimmer, J. Huw Davies
- Formal analysis: Abigail Plimmer
- Funding aquisition: J. Huw Davies
- Investigation: Abigail Plimmer
- Methodology: Abigail Plimmer
- Validation: Abigail Plimmer, J. Huw Davies
- Project Administration: J. Huw Davies, Abigail Plimmer
- Resources: J. Huw Davies
- Software: Abigail Plimmer, J. Huw Davies
- Supervision: J.Huw Davies, James Panton
- Writing - original draft: Abigail Plimmer
- Writing - review & editing: Abigail Plimmer, J. Huw Davies
- Visualisation: Abigail Plimmer

Appendix A Extended Data Tables

Table A1 Reference model initial conditions for simulation investigating the stability of basal mantle structures (BMSs).

Parameter	Symbol	Value	Units
Surface temperature	T_s	300	K
CMB temperature	T_{CMB}	4000	K
Internal heating rate	H	4.0 x 10^{-12}	W kg^{-1}
Reference density	ρ	4500	kg m^{-3}
Gravitational acceleration	g	10	m s^{-2}
Thermal conductivity	k	4	$Wm^{-1}K^{-1}$
Specific heat capacity	C_p	1000	$JK^{-1}kg^{-1}$
Reference viscosity	μ_0	4.0 x 10^{21}	Pa s
Thermal expansivity	α	2.5 x 10^{-5}	K^{-1}
Lithosphere viscosity multiplication factor	$\Delta\mu_{li}$	100	-
Lower mantle viscosity multiplication factor	$\Delta\mu_{LM}$	30	-
Viscosity - depth dependence	Va	1	-
Viscosity - temperature dependence	Ea	1.5	-
Basally heated Rayleigh number	Ra_H	$\approx 3 \times 10^6$	-
Internally heated Rayleigh number	Ra_H	$\approx 5 \times 10^7$	-

Table A2 Molar compositions of three particle lithologies (harzburgite, lherzolite, and basalt)[24]

	Harzburgite	Lherzolite	Basalt
SiO_2	36.184	38.819	52.298
MgO	56.559	49.894	15.812
FeO	5.954	6.145	7.121
CaO	0.889	2.874	13.027
Al_2O_3	0.492	1.963	2.244

Table A3 Parameter space for suite of models where models 000-004 have varying CMB temperature, 005-007 have varying plate velocity at the surface, 008-013 have different viscosity structures, 014-016 have different thickness of a basal primordial layer, 017-019 changes the density of a 300 km thick primordial layer, and 020-023 implement different plate motion histories with different reference frames.

Model No	CMB temp. (K)	Plate vel. (cm/yr)	Visc. profile	Primordial layer thickness	Density of primordial layer	Plate motion history
Ref	4000	2.3	v1	-	-	Mu
001	4250	2.3	v1	-	-	Mu
002	4500	2.3	v1	-	-	Mu
003	3500	2.3	v1	-	-	Mu
004	3000	2.3	v1	-	-	Mu
005	4000	9.1	v1	-	-	Mu
006	4000	4.5	v1	-	-	Mu
007	4000	1.5	v1	-	-	Mu
008	4000	2.3	v2	-	-	Mu
009	4000	2.3	v3	-	-	Mu
010	4000	2.3	v4	-	-	Mu
011	4000	2.3	v5	-	-	Mu
012	4000	2.3	v6	-	-	Mu
013	4000	2.3	v7	-	-	Mu
014	4000	2.3	v1	150	3%	Mu
015	4000	2.3	v1	300	3%	Mu
016	4000	2.3	v1	75	3%	Mu
017	4000	2.3	v1	150	1%	Mu
018	4000	2.3	v1	150	5%	Mu
019	4000	2.3	v1	150	10%	Mu
020	4000	2.3	v1	-	-	Me
021	4000	2.3	v1	-	-	NNR
022	4000	2.3	v1	-	-	OV
023	4000	2.3	v1	-	-	SSL

Appendix B Extended Data Figures

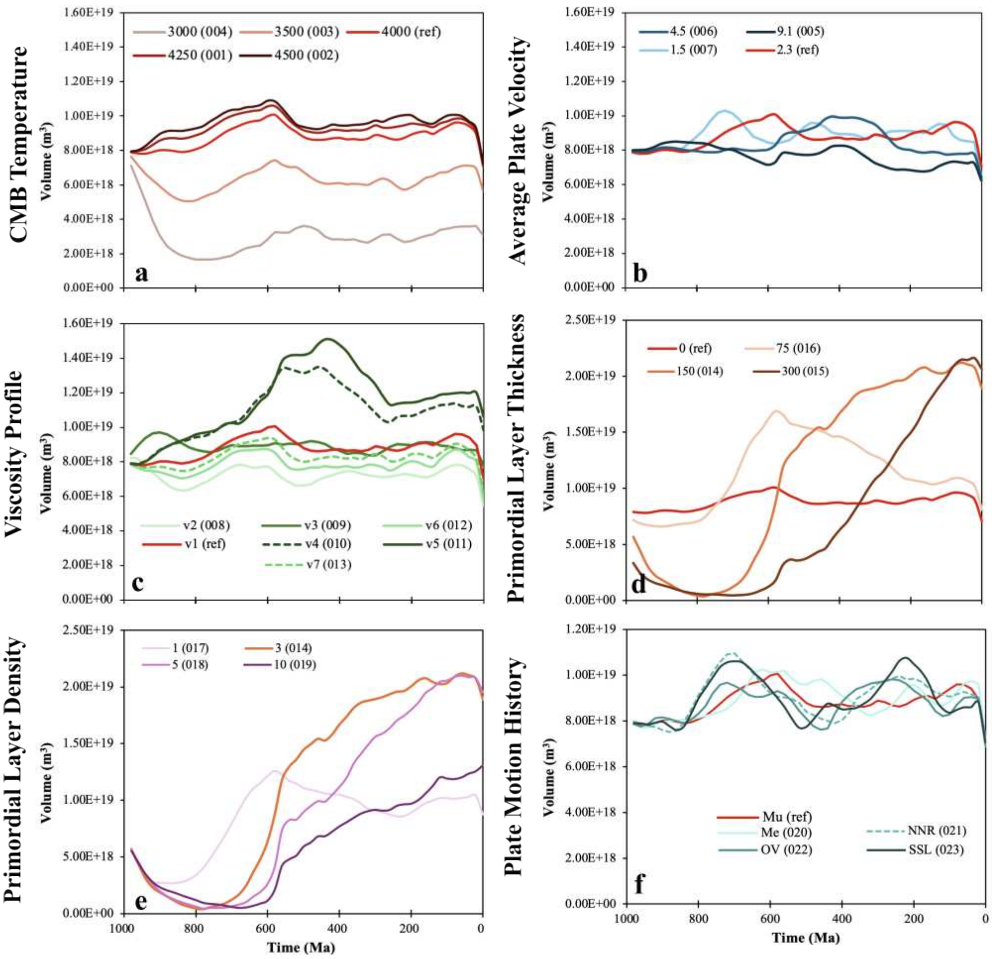

Fig. B1 Volumes of material defined as LLSVP-like in the lowermost 800 km of the mantle across each simulation, grouped by the varying parameter (CMB temperature, average plate velocity, viscosity profile, primordial layer thickness, primordial layer density, and plate motion reconstruction).

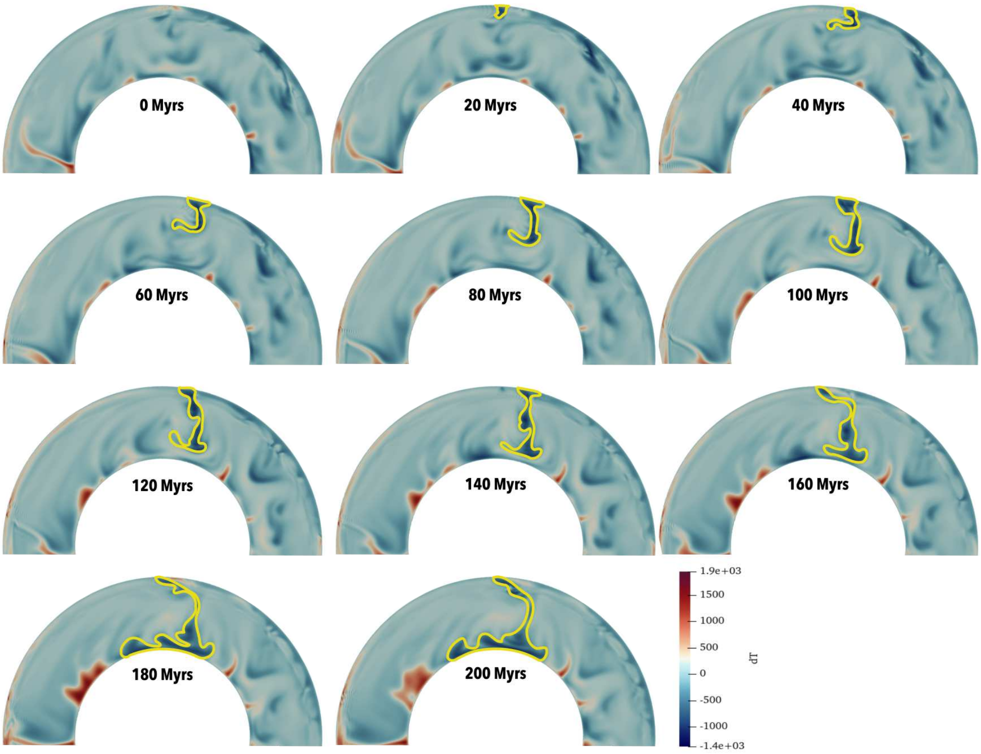

Fig. B2 Example slab (defined in yellow by -300 K thermal anomaly) in reference model, showing the time taken to sink through the mantle. Additionally, hot material is shown to be mobile about the CMB and migrates away from slabs as they sink.

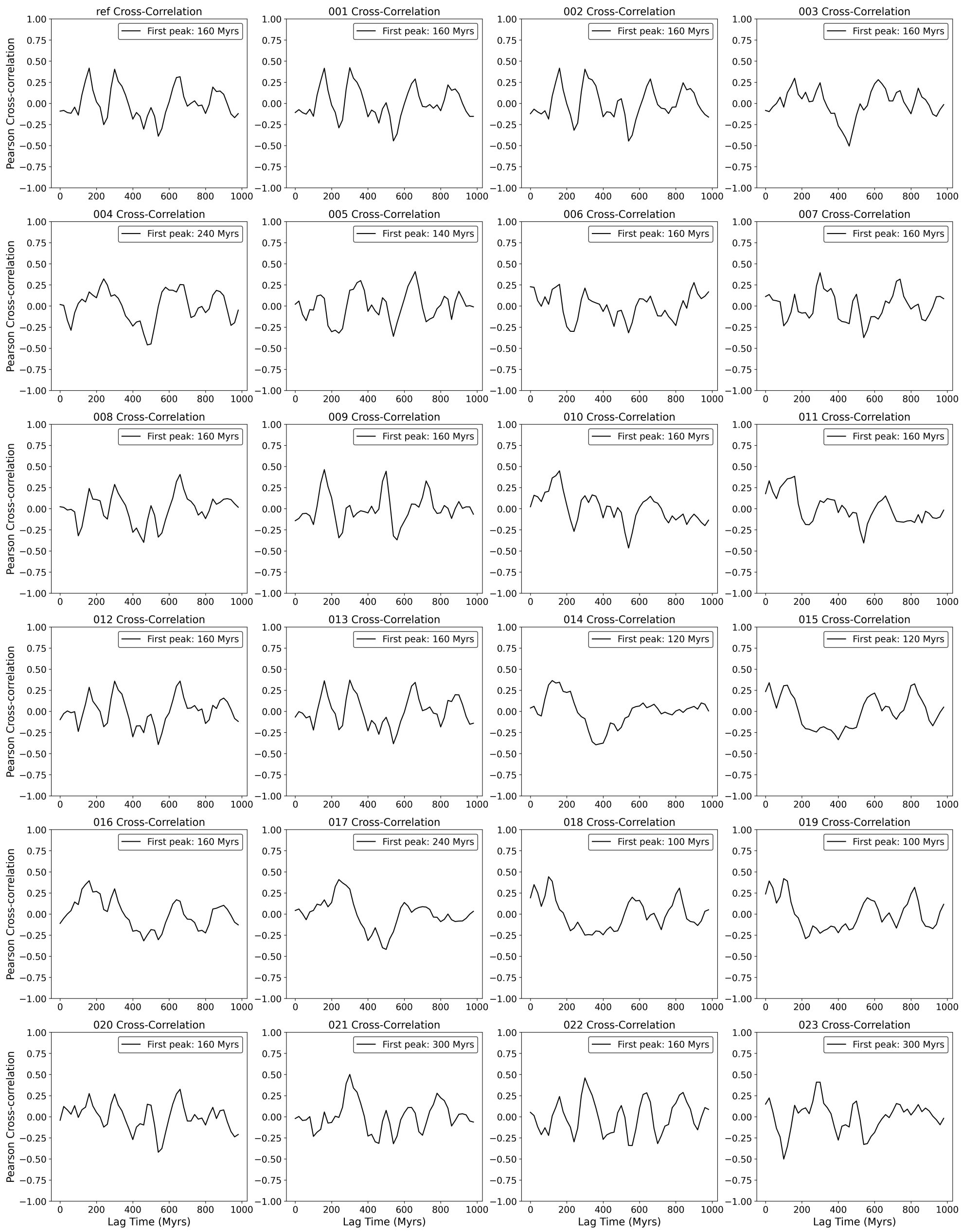

Fig. B3 Results of cross correlation algorithm for each simulation showing cycling trend in positive correlations and lag time of the first significant peak in Pearson cross-correlation value. Cross-correlations for each model compare the relationship between the change in volume and the global length of subduction zones. Significant peaks are defined by positive Pearson correlation coefficients and a prominence threshold of 0.2.

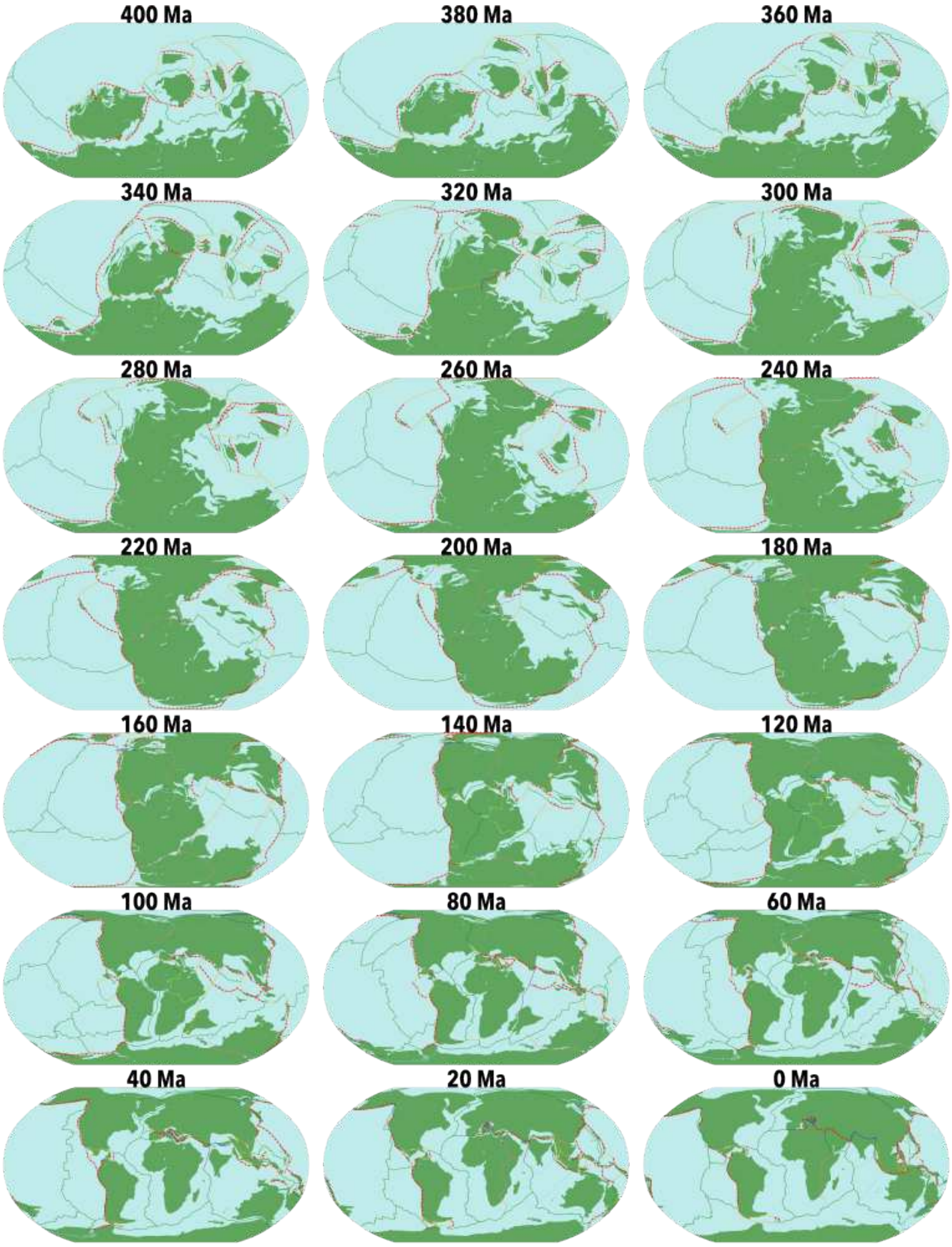

Fig. B4 Global GPlates [97] reconstruction through time from the plate motion history of [48] showing the evolution of subduction zones, and their relative stability between ∼ 320-100 Ma initially surrounding Pangaean supercontinent, and evolving into the Pacific Ring of Fire. Red - subduction zones, green - spreading ridges.

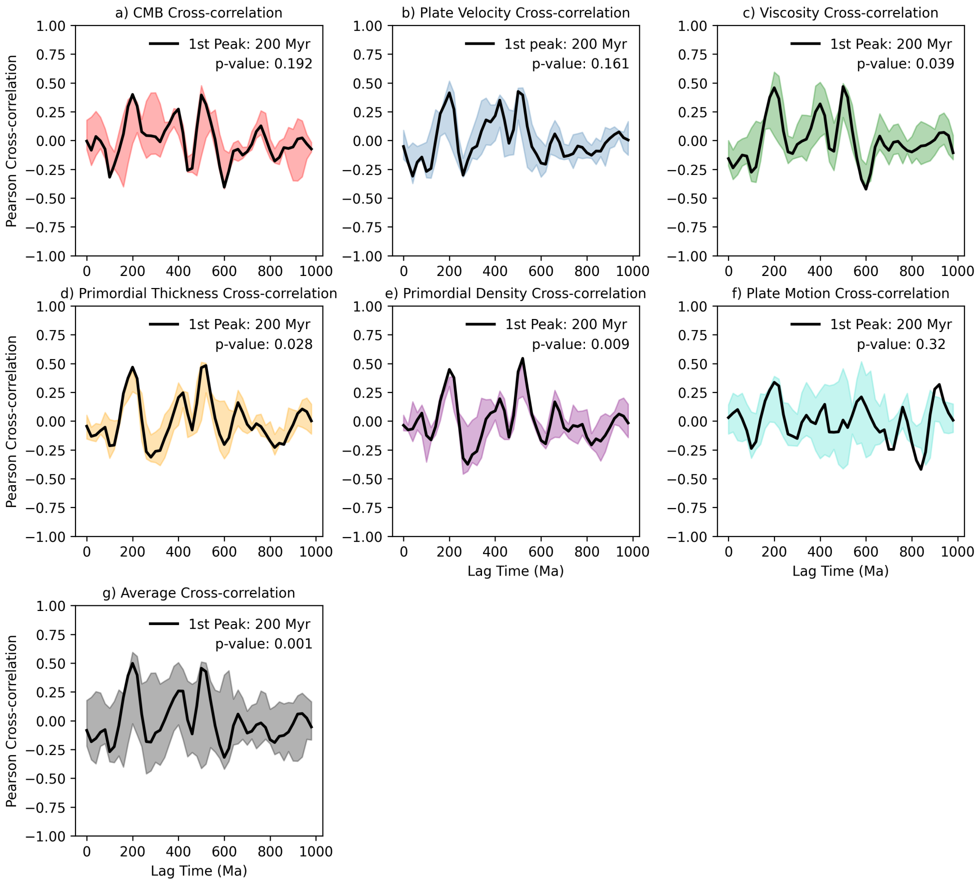

Fig. B5 Results of cross-correlation algorithm showing the relationship between global length of subduction zones and the change in dominant spherical harmonic degree across basal mantle structures through time. (a-f) Black lines show the average cross-correlation for models with different CMB temperatures, plate velocities, viscosities, primordial layer thicknesses, primordial layer densities, and plate motion histories, respectively. Coloured space represents the range of values across each individual model. g) average across all of the models. P-values are calculated from Monte-Carlo simulation with 1000 iterations.

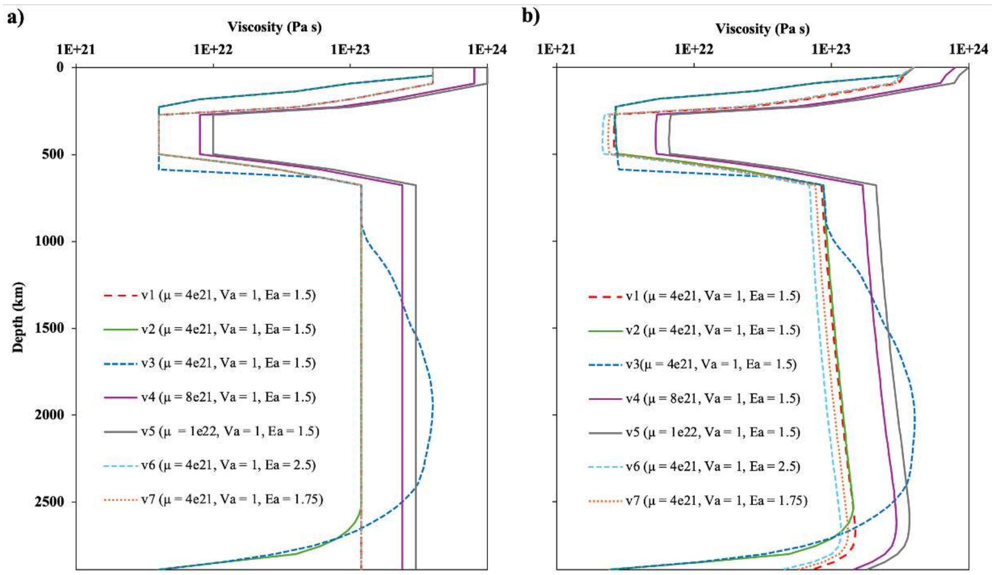

Fig. B6 7 different viscosity profiles used throughout the parameter space of this study at (a) the beginning of the simulations and (b) at the end of the simulations, once the effect of temperature dependence is more developed.

References

[1] Arnould, M., Coltice, N., Flament, N. & Mallard, C. Plate tectonics and mantle controls on plume dynamics. *Earth and Planetary Science Letters* **547**, 116439 (2020).

[2] Burke, K. Plate Tectonics, the Wilson cycle, and mantle plumes: Geodynamics from the top. *Annual Review of Earth and Planetary Sciences* **39**, 1–29 (2011).

[3] Davies, G. F. Whole-mantle convection and plate tectonics. *Geophysical Journal International* **49**, 459–486 (1977).

[4] Jellinek, A. M. & Manga, M. Links between long-lived hot spots, mantle plumes, D”, and plate tectonics. *Reviews of Geophysics* **42** (2004).

[5] Silver, P. G., Carlson, R. W. & Olson, P. Deep slabs, geochemical heterogeneity, and the large-scale structure of mantle convection: Investigation of an enduring paradox. *Annual Review of Earth and Planetary Sciences* **16**, 477 (1988).

[6] Yoshida, M. & Santosh, M. Supercontinents, mantle dynamics and plate tectonics: A perspective based on conceptual vs. numerical models. *Earth-Science Reviews* **105**, 1–24 (2011).

[7] Zhao, D. Global tomographic images of mantle plumes and subducting slabs: insight into deep earth dynamics. *Physics of the Earth and Planetary Interiors* **146**, 3–34 (2004).

[8] Dziewonski, A. M., Hager, B. H. & O'Connell, R. J. Large-scale heterogeneities in the lower mantle. *Journal of Geophysical Research (1896-1977)* **82**, 239–255 (1977).

[9] Garnero, E. J., McNamara, A. K. & Shim, S.-H. Continent-sized anomalous zones with low seismic velocity at the base of Earth's mantle. *Nature Geoscience* **9**, 481–489 (2016).

[10] Burke, K., Steinberger, B., Torsvik, T. H. & Smethurst, M. A. Plume Generation Zones at the margins of Large Low Shear Velocity Provinces on the core–mantle boundary. *Earth and Planetary Science Letters* **265**, 49–60 (2008).

[11] Ganerød, M. *et al.* The North Atlantic Igneous Province reconstructed and its relation to the plume generation zone: the Antrim Lava Group revisited. *Geophysical Journal International* **182**, 183–202 (2010).

[12] Ganerød, M. *et al.* Palaeoposition of the Seychelles microcontinent in relation to the Deccan traps and the Plume Generation Zone in late Cretaceous-early Palaeogene time. *Geological Society, London, Special Publications* **357**, 229–252 (2011).

[13] Heron, P. J. Mantle plumes and mantle dynamics in the Wilson cycle. *Geological Society, London, Special Publications* **470**, 87–103 (2019).

[14] McNamara, A. K. A review of large low shear velocity provinces and ultra low velocity zones. *Tectonophysics* **760**, 199–220 (2019).

[15] O'Connor, J., Jokat, W., Wijbrans, J. & Colli, L. Hotspot tracks in the south Atlantic located above bands of fast flowing asthenosphere driven by waning pulsations from the African LLSVP. *Gondwana Research* **53**, 197–208 (2018).

[16] Davies, D. R. *et al.* Reconciling dynamic and seismic models of Earth's lower mantle: The dominant role of thermal heterogeneity. *Earth and Planetary Science Letters* **353-354**, 253–269 (2012).

[17] Davies, D. R., Goes, S. & Lau, H. C. P. in *Thermally dominated deep mantle LLSVPs: A review* (eds Khan, A. & Deschamps, F.) *The Earth's Heterogeneous Mantle: A Geophysical, Geodynamical, and Geochemical Perspective* 441–477 (Springer International Publishing, 2015).

[18] Ritsema, J., McNamara, A. K. & Bull, A. L. Tomographic filtering of geodynamic models: Implications for model interpretation and large-scale mantle structure. *Journal of Geophysical Research: Solid Earth* **112** (2007).

[19] Schuberth, B. S. A., Bunge, H.-P. & Ritsema, J. Tomographic filtering of high-resolution mantle circulation models: Can seismic heterogeneity be explained by temperature alone? *Geochemistry, Geophysics, Geosystems* **10** (2009).

[20] Tackley, P. J. Dynamics and evolution of the deep mantle resulting from thermal, chemical, phase and melting effects. *Earth-Science Reviews* **110**, 1–25 (2012).

[21] Bower, D. J., Gurnis, M. & Seton, M. Lower mantle structure from paleogeographically constrained dynamic Earth models. *Geochemistry, Geophysics, Geosystems* **14**, 44–63 (2013).

[22] Bull, A., McNamara, A. & Ritsema, J. Synthetic tomography of plume clusters and thermochemical piles. *Earth and Planetary Science Letters* **278**, 152–162 (2009).

[23] Lassak, T. M., McNamara, A. K. & Zhong, S. Influence of thermochemical piles on topography at Earth's core–mantle boundary. *Earth and Planetary Science Letters* **261**, 443–455 (2007).

[24] Panton, J., Davies, J. H. & Myhill, R. The stability of dense oceanic crust near the core-mantle boundary. *Journal of Geophysical Research: Solid Earth* **128**, e2022JB025610 (2023).

[25] Yuan, Q. & Li, M. Instability of the African large low-shear-wave-velocity province due to its low intrinsic density. *Nature Geoscience* **15** (2022).

[26] Panton, J., Davies, J. H., Koelemeijer, P., Myhill, R. & Ritsema, J. Unique composition and evolutionary histories of large low velocity provinces. *Scientific Reports* **15**, 4466 (2025). URL https://doi.org/10.1038/s41598-025-88931-3.

[27] Le Bars, M. & Davaille, A. Whole layer convection in a heterogeneous planetary mantle. *Journal of Geophysical Research: Solid Earth* **109** (2004). URL https://agupubs.onlinelibrary.wiley.com/doi/abs/10.1029/2003JB002617.

[28] Olson, P. & Amit, H. Mantle superplumes induce geomagnetic superchrons. *Frontiers in Earth Science* **3**, 38 (2015).

[29] Gamal El Dien, H., Doucet, L. S., Li, Z.-X., Cox, G. & Mitchell, R. Global geochemical fingerprinting of plume intensity suggests coupling with the supercontinent cycle. *Nature Communications* **10**, 5270 (2019).

[30] McNamara, A. K. & Zhong, S. Thermochemical structures beneath Africa and the Pacific ocean. *Nature* **437**, 1136–1139 (2005).

[31] Heyn, B. H., Conrad, C. P. & Trønnes, R. G. How thermochemical piles can (periodically) generate plumes at their edges. *Journal of Geophysical Research: Solid Earth* **125**, e2019JB018726 (2020).

[32] Torsvik, T. H., Smethurst, M. A., Burke, K. & Steinberger, B. Long term stability in deep mantle structure: Evidence from the 300 Ma Skagerrak-Centered Large Igneous Province (the SCLIP). *Earth and Planetary Science Letters* **267**, 444–452 (2008).

[33] Conrad, C. P., Steinberger, B. & Torsvik, T. H. Stability of active mantle upwelling revealed by net characteristics of plate tectonics. *Nature* **498**, 479–482 (2013).

[34] Huang, C., Leng, W. & Wu, Z. Iron-spin transition controls structure and stability of LLSVPs in the lower mantle. *Earth and Planetary Science Letters* **423**, 173–181 (2015).

[35] Huang, C., Leng, W. & Wu, Z. The continually stable subduction, iron-spin transition, and the formation of LLSVPs from subducted oceanic crust. *Journal of Geophysical Research: Solid Earth* **125**, e2019JB018262 (2020).

[36] Mulyukova, E., Steinberger, B., Dabrowski, M. & Sobolev, S. V. Survival of LLSVPs for billions of years in a vigorously convecting mantle: Replenishment and destruction of chemical anomaly. *Journal of Geophysical Research: Solid Earth* **120**, 3824–3847 (2015).

[37] Davaille, A. & Romanowicz, B. Deflating the LLSVPs: Bundles of mantle thermochemical plumes rather than thick stagnant "piles". *Tectonics* **39**, e2020TC006265 (2020).

[38] MacLeod, S. J., Müller, R. D., Hassan, R. & Williams, S. E. in *Chapter 18 - evolution of mantle plumes and lower mantle structure in numerical models using tectonic reconstructions as boundary conditions* (ed.Duarte, J. C.) *Dynamics of Plate Tectonics and Mantle Convection* 427–458 (Elsevier, 2023).

[39] Zhang, N., Zhong, S., Leng, W. & Li, Z.-X. A model for the evolution of the Earth's mantle structure since the Early Paleozoic. *Journal of Geophysical Research: Solid Earth* **115** (2010).

[40] Zhong, S. & Rudolph, M. L. On the temporal evolution of long-wavelength mantle structure of the Earth since the early Paleozoic. *Geochemistry, Geophysics, Geosystems* **16**, 1599–1615 (2015).

[41] Li, Z.-X. & Zhong, S. Supercontinent-superplume coupling, true polar wander and plume mobility: Plate dominance in whole-mantle tectonics. *Physics of the Earth and Planetary interiors* **176**, 143–156 (2009).

[42] Cao, X., Flament, N. & Müller, R. D. Coupled evolution of plate tectonics and basal mantle structure. *Geochemistry, Geophysics, Geosystems* **22**, e2020GC009244 (2021).

[43] Cao, X., Flament, N., Bodur, F. & Müller, R. D. The evolution of basal mantle structure in response to supercontinent aggregation and dispersal. *Scientific Reports* **11**, 22967 (2021).

[44] Shi, Z. *et al.* Sluggish thermochemical basal mantle structures support their long-lived stability. *Nature Communications* **15**, 10000 (2024).

[45] Zhong, S., Zhang, N., Li, Z.-X. & Roberts, J. H. Supercontinent cycles, true polar wander, and very long-wavelength mantle convection. *Earth and Planetary Science Letters* **261**, 551–564 (2007).

[46] Doucet, L. S. *et al.* Coupled supercontinent-mantle plume events evidenced by oceanic plume record. *Geology* **48**, 159–163 (2020).

[47] Davies, G. F. *Perspective; Imperfect but Better Than Shouting*, 193–200 (Springer International Publishing, Cham, 2022). URL https://doi.org/10.1007/978-3-030-91359-5_16.

[48] Müller, R. D. *et al.* A tectonic-rules-based mantle reference frame since 1 billion years ago–implications for supercontinent cycles and plate–mantle system evolution. *Solid Earth* **13**, 1127–1159 (2022).

[49] Creager, K. C. & Jordan, T. H. Aspherical structure of the core-mantle boundary from PKP travel times. *Geophysical Research Letters* **13**, 1497–1500 (1986).

[50] Morelli, A. & Dziewonski, A. M. Topography of the core-mantle boundary and lateral homogeneity of the liquid core. *Nature* **325**, 678–683 (1987).

[51] Obayashi, M. & Fukao, Y. P and PcP travel time tomography for the core-mantle boundary. *Journal of Geophysical Research: Solid Earth* **102**, 17825–17841 (1997).

[52] Boschi, L. & Dziewonski, A. M. Whole Earth tomography from delay times of P, PcP, and PKP phases: Lateral heterogeneities in the outer core or radial anisotropy in the mantle? *Journal of Geophysical Research: Solid Earth* **105**, 13675–13696 (2000).

[53] Sze, E. K. & van der Hilst, R. D. Core mantle boundary topography from short period PcP, PKP, and PKKP data. *Physics of the Earth and Planetary Interiors* **135**, 27–46 (2003).

[54] Tanaka, S. Constraints on the core-mantle boundary topography from P4KP-PcP differential travel times. *Journal of Geophysical Research: Solid Earth* **115** (2010). URL https://agupubs.onlinelibrary.wiley.com/doi/abs/10.1029/2009JB006563.

[55] Lassak, T. M., McNamara, A. K., Garnero, E. J. & Zhong, S. Core–mantle boundary topography as a possible constraint on lower mantle chemistry and

dynamics. *Earth and Planetary Science Letters* **289**, 232–241 (2010). URL https://www.sciencedirect.com/science/article/pii/S0012821X09006591.

[56] Koelemeijer, P. J., Deuss, A. & Trampert, J. Normal mode sensitivity to Earth's D" layer and topography on the core-mantle boundary: what we can and cannot see. *Geophysical Journal International* **190**, 553–568 (2012). URL https://doi.org/10.1111/j.1365-246X.2012.05499.x.

[57] Steinberger, B. & Torsvik, T. H. A geodynamic model of plumes from the margins of large low shear velocity provinces. *Geochemistry, Geophysics, Geosystems* **13** (2012). URL https://agupubs.onlinelibrary.wiley.com/doi/abs/10.1029/2011GC003808.

[58] Li, M. & Zhong, S. The source location of mantle plumes from 3D spherical models of mantle convection. *Earth and Planetary Science Letters* **478**, 47–57 (2017). URL https://www.sciencedirect.com/science/article/pii/S0012821X17304806.

[59] Hassan, R., Flament, N., Gurnis, M., Bower, D. J. & Müller, D. Provenance of plumes in global convection models. *Geochemistry, Geophysics, Geosystems* **16**, 1465–1489 (2015).

[60] Plimmer, A., Davies, J. H. & Panton, J. Investigating the effect of lithosphere thickness and viscosity on mantle dynamics throughout the supercontinent cycle. *Geochemistry, Geophysics, Geosystems* **25**, e2024GC011688 (2024). URL https://agupubs.onlinelibrary.wiley.com/doi/abs/10.1029/2024GC011688.

[61] Schellart, W., Strak, V., Beniest, A., Duarte, J. & Rosas, F. Subduction invasion polarity switch from the Pacific to the Atlantic Ocean: A new geodynamic model of subduction initiation based on the Scotia Sea region. *Earth-Science Reviews* **236**, 104277 (2023).

[62] Gutscher, M.-A. *et al.* The Gibraltar subduction: A decade of new geophysical data. *Tectonophysics* **574**, 72–91 (2012).

[63] Duarte, J. C. *et al.* Are subduction zones invading the Atlantic? evidence from the southwest Iberia margin. *Geology* **41**, 839–842 (2013).

[64] Duarte, J. C., Schellart, W. P. & Rosas, F. M. The future of Earth's oceans: consequences of subduction initiation in the Atlantic and implications for supercontinent formation. *Geological Magazine* **155**, 45–58 (2018).

[65] Duarte, J. C. *et al.* Gibraltar subduction zone is invading the Atlantic. *Geology* **52**, 331–335 (2024).

[66] Heron, P. J. *et al.* The impact of Pangean subducted oceans on mantle dynamics: Passive piles and the positioning of deep mantle plumes. *Gondwana Research* **138**, 168–185 (2025). URL https://www.sciencedirect.com/science/article/pii/

S1342937X24002910.

[67] Wang, Y. & Li, M. Constraining mantle viscosity structure from a statistical analysis of slab stagnation events. *Geochemistry, Geophysics, Geosystems* **21**, e2020GC009286 (2020).

[68] Condie, K. C. Episodic continental growth and supercontinents: a mantle avalanche connection? *Earth and Planetary Science Letters* **163**, 97–108 (1998).

[69] Puetz, S. J., Spencer, C. J. & Ganade, C. E. Analyses from a validated global upb detrital zircon database: Enhanced methods for filtering discordant upb zircon analyses and optimizing crystallization age estimates. *Earth-Science Reviews* **220**, 103745 (2021). URL https://www.sciencedirect.com/science/article/pii/S0012825221002464.

[70] Baumgardner, J. R. Three-dimensional treatment of convective flow in the Earth's mantle. *Journal of Statistical Physics* **39**, 501–511 (1985).

[71] Bunge, H. & Baumgardner, J. R. Mantle convection modeling on parallel virtual machines. *Computers in physics* **9**, 207–215 (1995).

[72] Bunge, H., Richards, M. A. & Baumgardner, J. R. A sensitivity study of three-dimensional spherical mantle convection at 10^8 Rayleigh number: Effects of depth-dependent viscosity, heating mode, and an endothermic phase change. *Journal of Geophysical Research: Solid Earth* **102**, 11991–12007 (1997).

[73] Davies, D. R. *et al.* A hierarchical mesh refinement technique for global 3-D spherical mantle convection modelling. *Geoscientific Model Development* **6**, 1095–1107 (2013).

[74] Yang, W.-S. & Baumgardner, J. R. A matrix-dependent transfer multigrid method for strongly variable viscosity infinite Prandtl number thermal convection. *Geophysical & Astrophysical Fluid Dynamics* **92**, 151–195 (2000).

[75] Baumgardner, J. R. & Frederickson, P. O. Icosahedral discretization of the two-sphere. *SIAM Journal on Numerical Analysis* **22**, 1107–1115 (1985).

[76] Jarvis, G. T. & Mckenzie, D. P. Convection in a compressible fluid with infinite prandtl number. *Journal of Fluid Mechanics* **96**, 515–583 (1980).

[77] Hager, B. H., Clayton, R. W., Richards, M. A., Comer, R. P. & Dziewonski, A. M. Lower mantle heterogeneity, dynamic topography and the geoid. *Nature* **313**, 541–545 (1985).

[78] Van Keken, P. E. & Ballentine, C. J. Whole-mantle versus layered mantle convection and the role of a high-viscosity lower mantle in terrestrial volatile evolution. *Earth and Planetary Science Letters* **156**, 19–32 (1998).

[79] Tetley, M. G., Williams, S. E., Gurnis, M., Flament, N. & Müller, R. D. Constraining absolute plate motions since the Triassic. *Journal of Geophysical Research: Solid Earth* **124**, 7231–7258 (2019).

[80] Price, M. G., Davies, J. H. & Panton, J. Controls on the deep-water cycle within three-dimensional mantle convection models. *Geochemistry, Geophysics, Geosystems* **20**, 2199–2213 (2019).

[81] Van Heck, H. J., Davies, J. H., Elliott, T. & Porcelli, D. Global-scale modelling of melting and isotopic evolution of Earth's mantle: melting modules for TERRA. *Geoscientific Model Development* **9**, 1399–1411 (2016).

[82] Baker, M. B. & Beckett, J. R. The origin of abyssal peridotites: a reinterpretation of constraints based on primary bulk compositions. *Earth and Planetary Science Letters* **171**, 49–61 (1999).

[83] Walter, M. in *2.08 - melt extraction and compositional variability in mantle lithosphere* (eds Holland, H. D. & Turekian, K. K.) *Treatise on Geochemistry* 363–394 (Pergamon, Oxford, 2003).

[84] White, W. & Klein, E. in *4.13 - composition of the oceanic crust* Second edition edn, (eds Holland, H. D. & Turekian, K. K.) *Treatise on Geochemistry (Second Edition)* 457–496 (Elsevier, Oxford, 2014).

[85] Panton, J. *et al.* Investigating influences on the pb pseudo-isochron using three-dimensional mantle convection models with a continental reservoir. *Geochemistry, Geophysics, Geosystems* **23**, e2021GC010309 (2022). URL https://agupubs.onlinelibrary.wiley.com/doi/abs/10.1029/2021GC010309. E2021GC010309 2021GC010309.

[86] Connolly, J. A. D. The geodynamic equation of state: What and how. *Geochemistry, Geophysics, Geosystems* **10** (2009).

[87] Stixrude, L. & Lithgow-Bertelloni, C. Thermal expansivity, heat capacity and bulk modulus of the mantle. *Geophysical Journal International* **228**, 1119–1149 (2021).

[88] Goes, S., Cammarano, F. & Hansen, U. Synthetic seismic signature of thermal mantle plumes. *Earth and Planetary Science Letters* **218**, 403–419 (2004).

[89] Maguire, R., Ritsema, J., van Keken, P. E., Fichtner, A. & Goes, S. P- and S-wave delays caused by thermal plumes. *Geophysical Journal International* **206**, 1169–1178 (2016).

[90] Matas, J. & Bukowinski, M. S. On the anelastic contribution to the temperature dependence of lower mantle seismic velocities. *Earth and Planetary Science Letters* **259**, 51–65 (2007). URL https://doi.org/10.1016/j.epsl.2007.04.028.

[91] Lay, T., Hernlund, J. & Buffett, B. A. Core-mantle boundary heat flow. *Nature geoscience* **1**, 25–32 (2008).

[92] Murakami, M., Khan, A., Sossi, P. A., Ballmer, M. D. & Saha, P. The composition of Earth's lower mantle. *Annual Review of Earth and Planetary Sciences* **52**, 605–638 (2024). URL https://www.annualreviews.org/content/journals/10.1146/annurev-earth-031621-075657.

[93] King, S. D. The viscosity structure of the mantle. *Reviews of Geophysics* **33**, 11–17 (1995).

[94] Merdith, A. S. *et al.* Extending full-plate tectonic models into deep time: Linking the Neoproterozoic and the Phanerozoic. *Earth-Science Reviews* **214**, 103477 (2021).

[95] Young, A. *et al.* Global kinematics of tectonic plates and subduction zones since the late Paleozoic era. *Geoscience Frontiers* **10**, 989–1013 (2019).

[96] Nowacki, A. *et al.* terratools: A python package to analyse TERRA mantle convection simulations. (2024).

[97] Müller, R. D. *et al.* Gplates: building a virtual Earth through deep time. *Geochemistry, Geophysics, Geosystems* **19**, 2243–2261 (2018).

[98] Ahrens, J., Geveci, B. & Law, C. in *ParaView: An end-user tool for large-data visualization* 717–731 (2005).

[99] Hunter, J. D. Matplotlib: A 2d graphics environment. *Computing in Science & Engineering* **9**, 90–95 (2007).